The Astrophysical Journal, 766:120 (16pp), 2013 April 1 doi:10.1088/0004-637X/766/2/120
© 2013. The American Astronomical Society. All rights reserved. Printed in the U.S.A.

THE THREE-DIMENSIONAL STRUCTURE OF THE M31 SATELLITE SYSTEM; STRONG EVIDENCE FOR AN INHOMOGENEOUS DISTRIBUTION OF SATELLITES

A. R. Conn[1,2,3], G. F. Lewis[4], R. A. Ibata[3], Q. A. Parker[1,2,5], D. B. Zucker[1,2,5], A. W. McConnachie[6], N. F. Martin[3,7], D. Valls-Gabaud[8], N. Tanvir[9], M. J. Irwin[10], A. M. N. Ferguson[11], and S. C. Chapman[12]

[1] Department of Physics & Astronomy, Macquarie University, NSW 2109, Australia
[2] Research Centre in Astronomy, Astrophysics and Astrophotonics (MQAAAstro), Macquarie University, NSW 2109, Australia
[3] Observatoire Astronomique de Strasbourg, Université de Strasbourg, CNRS, UMR 7550, 11 rue de l'Université, F-67000 Strasbourg, France
[4] Sydney Institute for Astronomy, School of Physics, A28, University of Sydney, Sydney NSW 2006, Australia
[5] Australian Astronomical Observatory, P.O. Box 296, Epping, NSW 2121, Australia
[6] NRC Herzberg Institute of Astrophysics, 5071 West Saanich Road, Victoria, British Columbia, V9E 2E7, Canada
[7] Max-Planck-Institut für Astronomie, Königstuhl 17, D-69117 Heidelberg, Germany
[8] Observatoire de Paris, LERMA, 61 Avenue de l'Observatoire, F-75014 Paris, France
[9] Department of Physics and Astronomy, University of Leicester, Leicester LE1 7RH, UK
[10] Institute of Astronomy, University of Cambridge, Madingley Road, Cambridge CB3 0HA, UK
[11] Institute for Astronomy, University of Edinburgh, Royal Observatory, Blackford Hill, Edinburgh EH9 3HJ, UK
[12] Department of Physics and Atmospheric Science, Dalhousie University, 6310 Coburg Road, Halifax, Nova Scotia, B3H 4R2, Canada
Received 2012 November 8; accepted 2013 January 29; published 2013 March 15

ABSTRACT

We undertake an investigation into the spatial structure of the M31 satellite system utilizing the distance distributions presented in a previous publication. These distances make use of the unique combination of depth and spatial coverage of the Pan-Andromeda Archaeological Survey to provide a large, homogeneous sample consisting of 27 of M31's satellites, as well as M31 itself. We find that the satellite distribution, when viewed as a whole, is no more planar than one would expect from a random distribution of equal size. A disk consisting of 15 of the satellites is however found to be highly significant, and strikingly thin, with an rms thickness of just $12.34^{+0.75}_{-0.43}$ kpc. This disk is oriented approximately edge-on with respect to the Milky Way and almost perpendicular to the Milky Way disk. It is also roughly orthogonal to the disk-like structure regularly reported for the Milky Way satellite system and in close alignment with M31's Giant Stellar Stream. A similar analysis of the asymmetry of the M31 satellite distribution finds that it is also significantly larger than one would expect from a random distribution. In particular, it is remarkable that 20 of the 27 satellites most likely lie on the Milky Way side of the galaxy, with the asymmetry being most pronounced within the satellite subset forming the aforementioned disk. This lopsidedness is all the more intriguing in light of the apparent orthogonality observed between the satellite disk structures of the Milky Way and M31.

Key words: galaxies: dwarf – galaxies: halos – galaxies: individual (M31) – galaxies: structure

Online-only material: color figures

1. INTRODUCTION

The possibility that irregular distributions of satellite galaxies may be a common feature of large galaxy halos was originally bolstered by several studies of the anisotropic distribution of our own galaxy's satellites. Lynden-Bell (1976) found that the Magellanic Stream along with Sculptor and the Draco-Ursa Minor Stream and their associated dwarf spheroidal galaxies all appear to lie in the orbital plane of the Magellanic Clouds. In Lynden-Bell (1982), all the then-known dwarf spheroidal companions of the Milky Way are identified as lying in one of two streams. Kroupa et al. (2005) examined the likelihood of producing the observed disk-like distribution of Milky Way satellites from a spherical or oblate dark matter halo. From comparisons with theoretical isotropic satellite distributions produced from such a halo, they find that the chance of producing the observed distribution from the dark-matter sub-halos of cold-dark-matter (CDM) cosmology is less than 0.5%. They examine various combinations of the inner most satellites and find a best-fit plane that is almost perpendicular to the plane of the Milky Way with an rms height ranging from only about 10–30 kpc. Zentner et al. (2005), while finding a similar plane to Kroupa et al. (2005) for the Milky Way satellites, disagree with their assumption that such a plane is unlikely to arise from a conventional CDM dark matter halo. They argue that that the most luminous satellites cannot be taken for granted as forming randomly from the isotropic sub-halo distribution but instead, lie preferentially at smaller distances from the halo center and co-planar with the major axis of the host halo. Coupled with the finding that galaxies preferentially align themselves with their major axis highly inclined or even perpendicular to that of the surrounding matter (e.g., Navarro et al. 2004; Hartwick 2000), this would provide a good explanation for the observed orientation of the best-fit plane. The arguments of Zentner et al. (2005) are contended by Metz et al. (2007), however, and it should be noted that in contrast to Zentner et al. (2005), Libeskind et al. (2005) found that the distribution of the most massive sub-halos is not as flattened as the distribution of the Milky Way's satellites.

More recently, Lovell et al. (2011), using the six halo models in the Aquarius Simulations (Springel et al. 2008), find that all six halos produce a significant population of sub-halos with quasi-planar orbits aligned with the main halo spin. This, they argue, is a natural explanation for the observed satellite distribution of the Milky Way. Pawlowski et al. (2012a) argue against this, however. With the calculation of the angular momenta of 8 Milky Way Satellites (Metz et al. 2008) revealing a strong alignment between six of the orbital poles, Pawlowski et al. (2012a) examine the likelihood of randomly drawing six sub-halos from each of the six Aquarius simulations (among other halo

simulations) and finding a similar degree of alignment. More precisely, they draw 10^5 sets of eight satellites from each of the six simulations, and select the six with the highest degree of alignment between their orbits, thus emulating the findings of Metz et al. (2008). They then look at the degree of clumping of the orbital poles $\Delta_{\rm sph}$ as well as the angular distance of the average of the orbital pole inclinations from the model equator d and find that the actual degree of planarity observed for the six satellites identified by Metz et al. (2008) ($\Delta_{\rm sph}^{\rm MW} = 35.^\circ4$ and $d_{\rm MW} = 9.^\circ4$) are equaled or exceeded in the random draws in less than 10% of cases when $\Delta_{\rm sph}$ is considered and less than 15% of cases for d. Starkenburg et al. (2013) also find that the degree of planarity observed for the Milky Way satellites is uncommon in all six of the Aquarius halos (see Figure 7 of that study).

In addition to the revelation that the Milky Way's satellites appear to inhabit highly inclined great planes, they also appear to corroborate the finding of Holmberg (1969), namely that the companions of Spiral Galaxies preferentially congregate at high galactic latitudes (the Holmberg Effect), as observed in his study of 174 galaxy groups. It is not clear why this should be the case, or even if it truly is the case, although if the apparent adherence of satellite systems to polar great planes is typical of galaxies in general, then the Holmberg Effect seems to be an extension of this. Quinn & Goodman (1986) proposed that dynamical friction may be responsible for the observed polar great planes, with those orbits spending the most time in close proximity to the galactic disk experiencing the fastest decay, while those that take the most direct route through the disk environs, namely the polar orbits, experience the slowest orbital decay. It should be noted however that dynamical friction, while producing more polar orbits, would not produce planes of satellites. Nor would it be effective on the young globular clusters which are shown to be co-planar with the "Vast Plane of Satellites" identified around the Milky Way by Pawlowski et al. (2012b). Indeed, Angus et al. (2011) show that dynamical friction did not play a role in the formation of the Milky Way satellite orbits.

Besides the conjecture that satellite great planes trace the major axis of the dark matter halo in which the parent galaxy resides, there are other proposed mechanisms for their creation. One hypothesis is that these planes trace the orbits of ancient galaxies that have been cannibalized by the host galaxy. Palma et al. (2002) have investigated this hypothesis by looking for planes among groups of satellite galaxies and globular clusters in the Milky Way's outer halo and find various members to be co-planar with either the Magellanic or Sagittarius streams. The findings of Lynden-Bell & Lynden-Bell (1995) are also consistent with such a hypothesis. Indeed, it is this hypothesis which is most strongly supported by Pawlowski et al. (2012a), wherein the $\Delta_{\rm sph}$ and d of satellites drawn from various tidal models equal or exceed $\Delta_{\rm sph}^{\rm MW}$ and $d_{\rm MW}$ in over 80% of draws in some cases. A similar hypothesis, which in some regards links the galaxy-cannibalization and dark-matter hypotheses, proposes that the observed planes result from the orientation of the large-scale filamentary structure of galaxy clusters (e.g., Knebe et al. 2004), an orientation traced out by those minor galaxies which fall into the halo of a major galaxy. Metz et al. (2009b) argue however that extragalactic associations of dwarf galaxies are too extended to account for the high degree of planarity observed for the Milky Way satellites. This argument is supported by the findings of Vera-Ciro et al. (2011) based on the Aquarius Simulations.

The great obstacle to a conclusive resolution of these issues is the lack of systems for which reliable spatial (and kinematic) data exists. While some such data does exist for large galaxy clusters such as Virgo and Coma, accurate 3D distributions of galaxies within their halo have for a long time been known only for our own galaxy's halo, ascertainable due to our central position within it. It has only been in recent times that a second system has opened up to us—that of our counterpart in the Local Group, M31. While various databases of photometry and other data have been available for M31 and some of its brighter companions for over a decade, it is the Pan-Andromeda Archaeological Survey (PAndAS—McConnachie et al. 2009)—a deep photometric, two-color survey providing a uniform coverage of the M31 halo out to approximately 150 kpc—that has provided a new level of detail for this system. It is from this survey that we obtained our distances to M31 and 27 of its companions, following the method developed in Conn et al. (2011, henceforth CLI11) and further adapted for this purpose in Conn et al. (2012, henceforth CIL12). The distances themselves and their associated uncertainty distributions are presented in CIL12 and it is these distributions that are utilized for all analysis contained in this paper.

With regard to previous studies of the anisotropy in the M31 satellite distribution, two investigations warrant consideration at this point. McConnachie & Irwin (2006), making use of Wide Field Camera photometry from the Isaac Newton Telescope in what was essentially the forerunner to the PAndAS Survey, focus on "Ghostly Streams" of satellite galaxies following a similar approach as Lynden-Bell & Lynden-Bell (1995) used for the Milky Way. In addition, they characterize the large degree of asymmetry in the satellite distribution, a feature also noted in CIL12, and examine the radial distribution of the satellites, noting a (statistically insignificant) larger average distance from M31 than that observed between the Milky Way and its satellites. They find a large number of candidate satellite streams, with some favoring the dwarf spheroidal members. Koch & Grebel (2006) utilize distance measurements from a variety of sources and focus particularly on planes of satellites and, while they do not find a particularly significant best-fit plane when their whole satellite sample is considered, it is rather interesting that they find a 99.7% statistical significance to their best-fit plane when the then-known dwarf spheroidal galaxies dominate their sample. Furthermore, this plane is near-polar—as has been observed for the Milky Way, although they find little support for the Holmberg Effect. Koch & Grebel (2006) utilize a particularly robust method in their search for high-significance planar fits to subsets of galaxies by considering every possible combination of a given number of satellites from their sample.

In the current study we employ a similar approach, but with the great advantage of having a considerably extended sample of galaxies in our sample, with all distances derived by the same method and from the same data as described in CLI11 and CIL12. (Distances are sampled from the distributions without the density prior applied—e.g., CIL12, Table 1, Column 2—while the best-fit distances are drawn from CIL12, Table 2, Column 4.) As a result, we are able to give full consideration to the effects of selection bias on the observed satellite distribution. This then presents an excellent opportunity to greatly improve our knowledge of the three-dimensional structure of the M31 satellite distribution, with important implications regarding the recent evolution of the system.

A breakdown of the structure of the paper is as follows. In Section 2, we outline our method for plane fitting (Section 2.1) and locating significant planes of satellites as well as the orientation, magnitude and significance of the asymmetry of

the distribution. A method for generating random realizations of satellites subject to the same selection biases as the real data is also discussed in this section (Section 2.2) as is the selection bias itself (Section 2.3). Section 3 then presents the results of applying these methods, first to the sample as a whole, and then to subsets of galaxies. Specifically, Section 3.1 presents a study of planarity within the satellite system when all satellites contribute to the determination of the best-fit plane; Section 3.2 examines the asymmetry in a similar way; Section 3.3 examines the orientations of planes of smaller subsets of satellites within the distribution; and Section 3.4 concludes this section with a determination of the significance of a "Great Plane" of satellites emerging from the preceding sections. Sections 4 and 5 then follow with discussion and conclusions.

Note that this paper was written in conjunction with a shorter contribution (Ibata et al. 2013, hereafter ILC13) which announced some of the key discoveries resulting from the analysis we present here. In particular, the process of identifying the member satellites of the "great plane" discussed in ILC13 is described here in more detail. In this analysis, however, we concern ourselves with the *spatial* structure of the satellite system only and so the reader should refer to ILC13 for the interesting insight provided by the addition of the velocity information.

2. METHOD

2.1. Plane Fitting

In order to find planes of satellites within the M31 satellite system, our first concern is to convert the satellite distances as presented in CIL12 into three-dimensional positions. To do this, we begin with an M31-centered, Cartesian coordinate system oriented such that the x and y axes lie in the M31 tangent plane with the z-axis pointed toward the Earth. Specifically, the x-axis corresponds to $\eta_{\rm tp} = 0$ which is the projection of M31's Declination onto the tangent plane. The y-axis then corresponds to $\xi_{\rm tp} = 0$—the projection of M31's right ascension onto the tangent plane. The z-axis then points along the Earth-to-M31 vector, with magnitude increasing with distance from Earth. This orientation can be seen in Figure 10(c) of CIL12. Thus,

$$\begin{aligned} x &= D_{\rm sat}\cos(\theta)\tan(\xi) \\ y &= D_{\rm sat}\sin(\eta) \\ z &= D_{\rm sat}\cos(\theta) - {\rm D_{M31}}, \end{aligned} \quad (1)$$

where $D_{\rm M31}$ and $D_{\rm sat}$ are the distances from Earth to M31 and from Earth to the satellite, respectively, θ is the angular separation on the sky between M31 and the satellite, and η and ξ are the real-angle equivalents of the tangent plane projection angles $\eta_{\rm tp}$ and $\xi_{\rm tp}$, respectively.

Next, we rotate this reference frame to the conventional M31 reference frame such that the positive z-axis points toward M31's north galactic pole[13] (i.e., $b_{\rm M31} = +90^\circ$) and the $l_{\rm M31} = 0^\circ$ meridian passes through the Earth. So as to be consistent with the earlier work of McConnachie & Irwin (2006), we have adopted the same values for M31's position angle (39.°8) and inclination (77.°5—de Vaucouleurs 1958). Each object is hence rotated by 39.°8 about the z-axis to counter the effect of its position angle, and then 77.°5 about the x-axis to account for M31's inclination. A final rotation of 90° about the z-axis is then necessary to bring $l_{\rm M31} = 0^\circ$ into alignment with the direction of Earth (which hence lies at $l_{\rm M31} = 0^\circ$, $b_{\rm M31} = -12.^\circ5$). The resulting spherical coordinates for each object in the sample are plotted onto an Aitoff-Hammer projection in Figure 1. This same figure also shows the uncertainties in position associated with each object, generated via sampling of the respective distance posterior probability distributions (PPDs) of each object and subsequent conversion of each drawn distance into a three-dimensional position.

With the satellites' positions determined in Cartesian coordinates, it is straightforward to determine the minimum distance of each satellite from a given plane as follows:

$$D_{\rm plane} = |ax + by + cz + d|, \quad (2)$$

where $D_{\rm plane}$ is the distance of a satellite at a point (x, y, z) from a plane whose normal vector is (a, b, c) and is of unit length. For simplicity, we invoke the reasonable requirement that all planes must pass through the center of M31 and so in our case, $d = 0$ and the plane normal vector points out from the center of M31. Hence, in order to find the best-fit or maximum significance plane to a set of satellites, we need simply minimize $D_{\rm plane}$ for the satellites to be fitted. This can be done via a variety of means, some of which are compared in the following section, but perhaps the most robust and the predominant method employed in this study, is that of minimizing the rms of the distances to the fitted satellites.

In order to measure the asymmetry of the satellite distribution about a given plane, we need only count the number of satellites on one side of the plane. To do this, we can simply remove the absolute value signs from Equation (2), so that the side of the plane on which a satellite lies can be determined by whether $D_{\rm plane}$ is positive or negative. The plane of maximum asymmetry is then taken to be that which divides the sample such that the difference in satellite counts for opposite sides of the plane is greatest.

Whether we wish to determine the best-fit plane through a sample of satellites or the plane of maximum asymmetry, we require a system by which a large number of planes can be tested on the sample so that the goodness of fit (or asymmetry) can be calculated for each. To do this, we define each tested plane by its normal vector or pole (a, b, c) so that Equation (2) can be applied directly. We then rotate this pole to different orientations around the sky in such a way as to "scan" the whole sphere evenly and at a suitably high resolution. In practice, we need to be able to apply this routine many thousands of times for a large number of samples and so a fast computational time is of the essence. To this end, for a given sample, our algorithm determines the desired plane following a two step procedure.

First, a low-resolution scan of the sphere is made to determine the approximate direction on the sky of the pole to the best-fit plane. Only half the sphere actually needs to be scanned since poles lying on the opposite hemisphere correspond to the identical planes flipped upside down. The low-resolution scan tests 2233 different poles across the hemisphere. A near-uniform coverage is achieved by decreasing the number of planes tested in proportion to the cosine of the latitude of the planes' pole. This prohibits what would otherwise be an increased coverage at the higher latitudes of the coordinate system. With the pole to the best-fit plane determined in low-resolution, a high-resolution search is then made around the identified coordinates at 10 times the resolution. In this way a pole can effectively be found at any of approximately 250,000 evenly spread locations on the hemisphere.

[13] Defined so as to point north in Equatorial coordinates.

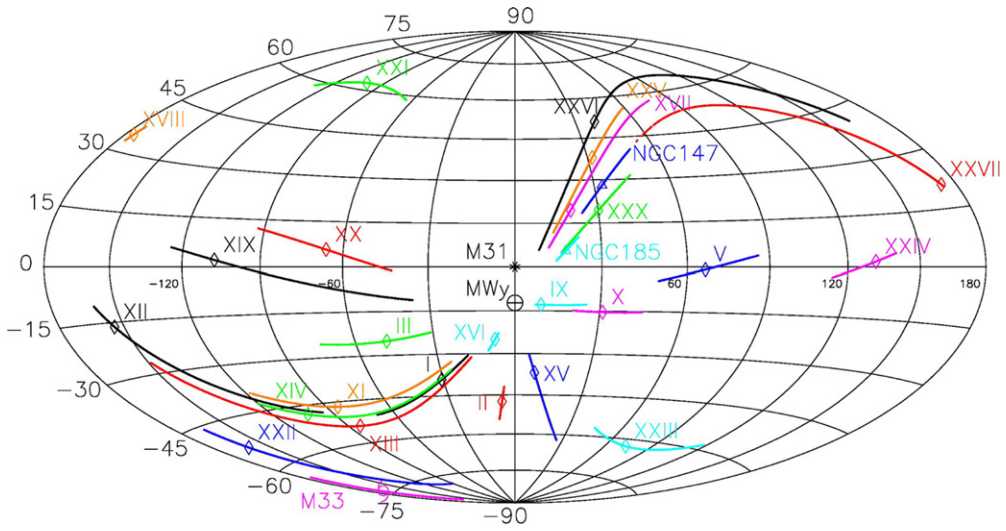

Figure 1. An Aitoff-Hammer Projection showing the positions of M31's satellites, along with their associated 1σ uncertainties. The positions show where each object would appear in the sky if viewed from the center of M31, and are given in M31's inherent galactic latitude and longitude. The position of the Milky Way is also shown for reference. The position uncertainties trace single arcs across the M31 sky, rather than two-dimensional patches on account of the restriction of the uncertainty to lie solely along the line of sight to the object from Earth. For this same reason, all the lines point radially outward from the Milky Way. These uncertainties also take into account the uncertainty in M31's distance. The existence of a prominent plane, broadly consisting of Andromedas I, XI, XII, XIII, XIV, XVI, XVII, XXV, XXVI, XXVII, XXX, and NGC 147 and NGC 185, is hinted at by the close proximity of their respective arcs.

(A color version of this figure is available in the online journal.)

2.2. Generating Random Satellite Samples

While we are now equipped to identify best-fit planes to our sample and subsamples thereof, it is necessary to have some means of determining the significance of these planes in an absolute sense. The most intuitive way to do this is to perform the same analysis on a randomly generated sample of equal size. In particular, when we are concerned with all possible combinations of a particular number of satellites that can be produced from the whole sample, we are often dealing with a very large number of subsamples and so it is inevitable that some of these subsets of satellites will exhibit a very high degree of planarity. Identical analysis must therefore be performed on random distributions, to see if there are similar numbers of subsets with equal degrees of planarity.

For this reason, considerable care was taken to design an algorithm capable of providing a unique random realization of the desired number of satellites whenever it is called. The algorithm makes use of the distance PPD for each satellite, and also takes into account the irregular window function (i.e., useable portion) of the PAndAS survey. Each time a satellite is to be added to the random realization, one of the 27 actual satellites is chosen at random and a distance is drawn from its associated PPD. This distance ($D_{\rm sat}$) is then converted into a three-dimensional position (x, y, z) following equation set 1 and this satellite-to-M31 separation vector is then spun around to a new, random location in the M31 sky. Note that for each random realization, a new value of $D_{\rm M31}$ is similarly drawn from the M31 distance PPD.

Once again, care must be taken in this step to ensure that the whole sphere is given equal weight, otherwise there is a higher likelihood for the artificial satellites to be positioned at high latitude. Again, this is remedied by weighting the likelihood by the cosine of the latitude.

With the new, random location for the satellite chosen, it is then projected back onto the sky as it would appear from Earth and a check is made to ensure that it does indeed lie within the boundaries of the PAndAS survey area, and outside of the central ellipse (5° major axis, 2° minor axis—see Figure 10(c) of CIL12) where the disk of M31 inhibits reliable measurements. If the satellite does not meet these requirements, it is rejected and the satellite drawing process is repeated until a suitable position is generated. By repeating this process until the desired number of satellites are produced, a new, random comparison sample is generated which gives full account to the constraints on the actual data.

In order for the random satellite realizations to mimic the actual data most closely, it is necessary that each artificial satellite is represented not by just one point, but rather a string of points reflecting the uncertainty in the Earth-to-Object distance. Hence once acceptable positions for each satellite are drawn as described above, the distance distributions for each object are sampled and projected to their equivalent positions along the line of sight about the initially placed point. For Sections 3.1, 3.2, and 3.4 each artificial satellite's distance distribution is represented by 1000 points such that each plane-fitting measurement is made for 1000 possible positions of the object and then the average value of the measurements is taken. The only exception to this number is where the maximum-likelihood approach is used in Section 3.1. Due to the inclusion of a second fitting parameter in this case, only 100 samples are taken for each satellite. For Section 3.3, as we are not concerned with comparisons of plane significance between the real sample and the random realizations, it is sufficient to use a single drawn position for each artificial satellite.

2.3. A Note on Satellite Detection Bias

By employing a similar method to that described above, it is also possible to explore the effect of the PAndAS survey area boundaries on the satellite detection bias as viewed from the center of M31. It is intuitive that more satellites are likely to be detected along the line of sight to Earth, since even satellites at a large distance from M31 will still appear within the survey boundaries if they lie along this line. We can visualize this effect by generating a large number of randomly distributed satellites

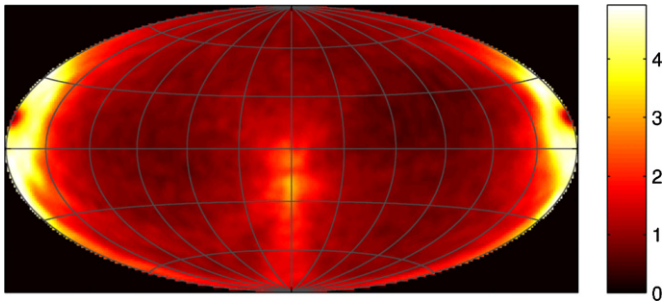

Figure 2. An Aitoff-Hammer projection illustrating the satellite detection bias resulting from the PAndAS survey boundaries and M31 disk obstruction. Note that this figure utilizes a Gaussian blurring of radius 5°, as do all of the subsequent pole-density plots.

(A color version of this figure is available in the online journal.)

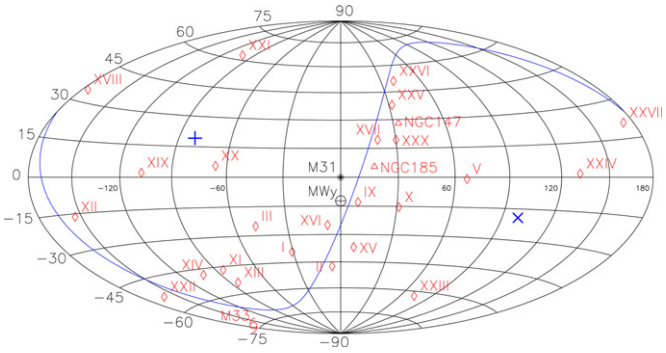

Figure 3. An Aitoff-Hammer Projection showing the best-fit plane to the satellite system as a whole. The pole and anti-pole of the plane are denoted by "+" and "×" symbols, respectively. Only the best-fit satellite positions were incorporated into the fit for this figure. The distribution of poles obtainable from other possible realizations of the satellite distribution is presented in Figure 4. Note that the plane is near-polar, similar to the preferred plane orientations identified for the Milky Way Satellite System.

(A color version of this figure is available in the online journal.)

and plotting them on the M31 sky after first rejecting those satellites that would appear outside the survey area "mask" if viewed from Earth. To do this, one million satellites were drawn from a spherically symmetric halo potential with density falling off as a function of the square of the distance from the halo center. Satellites were hence drawn at distances between 0 and 700 kpc from M31 with equal probability. The satellites were then projected onto the M31 tangent plane and those satellites lying outside the survey area or inside the M31 disk obstruction area were excised from the density map. The resulting anisotropy of the satellites on the M31 sky is presented in Figure 2.

As can be seen from the figure, the probability of detection is indeed higher along a great circle oriented edge-on with respect to the direction of Earth, and perpendicular to the M31 disk ($b_{\rm M31} = 0°$). This great circle has its pole/anti-pole at $l_{\rm M31} = \pm 90°, b_{\rm M31} = 0°$ and hence we would expect a predisposition toward finding planes of satellites with a pole in this vicinity. We would also expect, though to a lesser extent, to find an excess of satellite planes oriented edge-on with respect to Earth at any inclination. Such planes would have poles lying anywhere on the great circle whose normal is directed toward Earth. The drop in the satellite density at $l_{\rm M31} = 0°, b_{\rm M31} = -12.^{\circ}5$ and $l_{\rm M31} = \pm 180°, b_{\rm M31} = 12.^{\circ}5$ is a consequence of the hindrance to detection caused by the M31 disk. Due to the increased volume of space covered by the survey at greater distances from Earth, unhindered satellite detection is possible over a larger range of angles on the far side of M31 in comparison to the Earth-ward side.

3. RESULTS

3.1. Best-fit Plane to the Entire Satellite Sample

In order to find the best-fit plane to the satellite system as a whole, the procedure of Section 2.1 is applied to the whole sample of 27 satellites presented in CIL12. The rms thickness of the sample is used here, as in subsequent sections, as the statistic of planarity; we find it to be a robust measure and it has the convenient property of being computationally inexpensive. Since we are dealing with only one sample in this case, two other measures are also used for comparison. The first calculates the sum of the absolute values of the distances of each of the satellites from the tested plane. The second is essentially a maximum-likelihood approach and replaces the plane of zero-thickness with a "Gaussian Plane" such that a satellite's position within the Gaussian determines the plane's goodness of fit to that satellite. This second approach requires that different Gaussian widths σ be tested for each plane orientation in order to find the width that best matches the satellite distribution. Values between 5 kpc and 150 kpc were tested at 5 kpc intervals for each tested plane orientation. Hence an additional characteristic of the satellite distribution is obtained, but at the expense of a considerably longer computation time.

For each of the three measures of goodness of fit described above, the first step is to find the best-fit plane to the satellite positions with their positions determined from their best-fit distances. When either the rms or maximum-likelihood approach is used, the same best-fit plane is found as $0.153x + 0.932y + 0.329z = 0$ with pole at $(l_{\rm M31}, b_{\rm M31}) = (-80.^{\circ}7, 19.^{\circ}2)$. This plane is plotted as a great circle on the M31 sky in Figure 3 with the poles of the plane indicated. When the absolute distance sum is used instead, the pole is found farther from the plane of the galaxy, at $(l_{\rm M31}, b_{\rm M31}) = (-74.^{\circ}9, 24.^{\circ}3)$. Nevertheless, the polar plane described by Koch & Grebel (2006) is supported by either measurement, and is reminiscent of the satellite streams identified in the Milky Way satellite system. In light of the detection biases imposed by the PAndAS survey area as illustrated in Figure 2, the result in this case must clearly be treated with suitable caution, however. Like Koch & Grebel (2006), we find little evidence for the Holmberg Effect, with only three best-fit satellite positions falling within 30° of the M31 galactic poles, and only six of the 1σ error trails from Figure 1 pass beyond $b_{\rm M31} = \pm 60°$.

To determine the uncertainty in the plane's goodness of fit, we need to repeat the procedure for a large number of realizations of the satellite sample, with the best-fit satellite distances replaced with a distance drawn at random from their respective satellite distance PPDs. A density map of the best-fit plane poles identified from 200,000 such realizations is presented in Figure 4. This figure was generated using the distribution rms as the goodness of fit statistic, and contains 71.1% of all poles within a 5° radius of the best-fit pole stated above. When the sum of absolute distances is used in place of the rms, this fraction falls to 68.3%, or to 70.9% when the maximum-likelihood approach is used. It should be noted that the distribution of poles lies in close proximity to the pole of maximum detection bias at $l_{\rm M31} = -90°, b_{\rm M31} = 0°$, again suggesting that the detection bias is having a strong influence on the polar orientation of the best-fit plane.

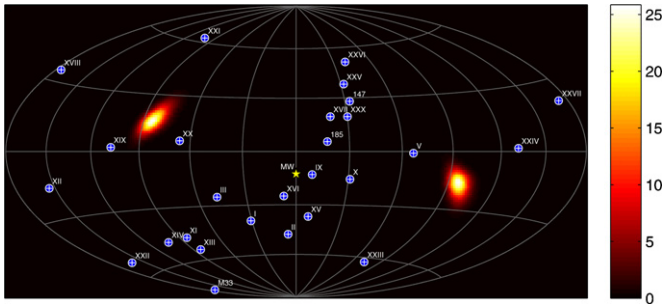

Figure 4. A pole density map showing the effective uncertainty in the location of the best-fit plane to the whole satellite sample. The poles of the best-fit planes derived for 200,000 possible realizations of the data are plotted, along with their corresponding anti-poles.

(A color version of this figure is available in the online journal.)

In order to determine whether the goodness of fit of the best-fit plane is really physically significant, similar analysis should be performed on a large number of random realizations of satellites, to see how often distributions of satellites arise with a comparable degree of planarity. Figure 5 presents probability distributions of the plane significance for possible realizations of the real satellite sample along with average values from random realizations of the satellites (as per Section 2.2), obtained using the three measures of goodness of fit stated above.

It is immediately clear from Figure 5 that regardless of the choice of the measure of goodness of fit, the range of values obtainable from possible realizations of the real satellite positions are similar to the most likely values to be expected from completely random realizations of the satellites. Hence, while a prominent plane of satellites comprising roughly half of the sample is suggested in Figure 1, it would seem that the sample as a whole is no more planar than would be expected from a strictly random distribution. Again, this is in keeping with the findings of Koch & Grebel (2006), and detracts from any physical significance that should be attributed to the plane's polar orientation.

Further to this finding, the overall width of the "plane" is again in keeping with that expected from a purely random satellite distribution. From fitting the Gaussian Plane to the best-fit satellite positions, a 1σ width of 60 kpc is found to produce the best fit to the data. When the 200,000 PPD-sampled realizations were tested, a 1σ of 60 kpc was found preferential in 66.3% of cases, with a 1σ of 55 kpc being preferred in 32.7% of cases. Values of 50 kpc make up the remaining 1% almost entirely. The average value for the actual satellite distribution was thus determined as 58.3 kpc. This value is similar to the most likely width identified from the 10,000 random realizations, as can be seen in Figure 6.

3.2. The Plane of Maximum Asymmetry

To determine the plane of maximum asymmetry and its significance, we employ an identical approach as in the preceding section, but with the goodness of fit statistic replaced with a count of the number of satellites on each side of the plane as per Section 2.1. As was suggested by the three-dimensional satellite distribution generated in CIL12, the asymmetry about the M31 tangent plane is close to a maximum, with 19 satellites on the near-side of the plane but only eight on the other when the best-fit satellite positions are assumed. The highest asymmetry plane possible from this same distribution has 21 satellites on one side and six on the other, with the equation of the plane identified by the algorithm as $-0.797x - 0.315y + 0.515z = 0$. The anti-pole of this plane lies 27.°2 away from the Milky Way at $(l_{\rm M31}, b_{\rm M31}) = (-21.°6, -31.°0)$. This plane is plotted as a great circle on the M31 sky in Figure 7.

When 200,000 realizations of the satellite sample are generated using the satellite's respective distance probability distributions, the most likely asymmetry of the sample is actually found to be greater than this, with 23 satellites on one side and only 4 on the other. Such a scenario is more than twice as likely as the 21:6 scenario. In one realization, a plane was identified which could divide the sample such that all 27 satellites lay in a single hemisphere, while an asymmetry of 26:1 was found possible for 815 (0.4%) of the realizations. The distribution of maximum-asymmetry poles on the sky, as determined from realizations of possible satellite positions, is illustrated in Figure 8, while Figure 9(a) plots the probability distribution for the greatest number of satellites that can be found in one hemisphere for a given realization of the observed satellite sample. The average value of this distribution is 22.7 (shown as a dashed line in Figure 9(b)), a value which is equaled or exceeded for 422 out of the 10,000 random realizations represented in Figure 9(b). A maximum asymmetry ratio of 21:6, as was observed for the best-fit satellite distribution plotted in Figure 7, is more common, however, falling inside the 1σ credibility interval.

What is particularly striking about the satellite distribution, however, is the orientation of the asymmetry, with the majority of satellites lying on the near-side of the M31 tangent plane. From Figure 9(c), it is clear that the effect of the distance uncertainties lying along the line of sight is to create quite a broad distribution in the level of asymmetry about the tangent plane, though the average is markedly high at 20.3. To investigate the likelihood of this scenario arising from a random satellite distribution, we measure the average number of satellites on either side of the M31 tangent plane for each of 10, 000 random realizations as per Section 2.2. The results are illustrated in Figure 9(d). The observed profile is more or less as expected, with a maximum probability close to the minimum possible asymmetry at 14 and then a rapid fall off toward higher asymmetries. It is therefore clear that the distance uncertainties lying along the line of sight have no significant bearing on the orientation of the asymmetry. Yet the observed degree of asymmetry about the M31 tangent plane is equaled or exceeded in only 46 of the 10,000 random satellite realizations and hence is very significant. The possibility that this asymmetry may be a consequence of data incompleteness is currently being examined more closely (see N. F. Martin 2013, in preparation), although it seems very unlikely. The high degree of asymmetry is still observed even when only the brightest satellites are considered. Furthermore, the data incompleteness appears to be dominated by the boundaries of the PAndAS survey area and obstructed regions which are already taken into account by our analysis. Indeed, one would expect more satellites to be observed on the far side of the M31 tangent plane on account of the increased volume of space covered by the survey at greater distances, an effect clearly visible in Figure 2.

3.3. Subsets of Satellites

It is perhaps not surprising that the satellite system of M31, when treated as a whole, is no more planar than one would expect from a random sample of comparable size. Indeed, a similar result was noted for the M31 system by Koch & Grebel (2006). The existence of outliers in our satellite sample was already clear

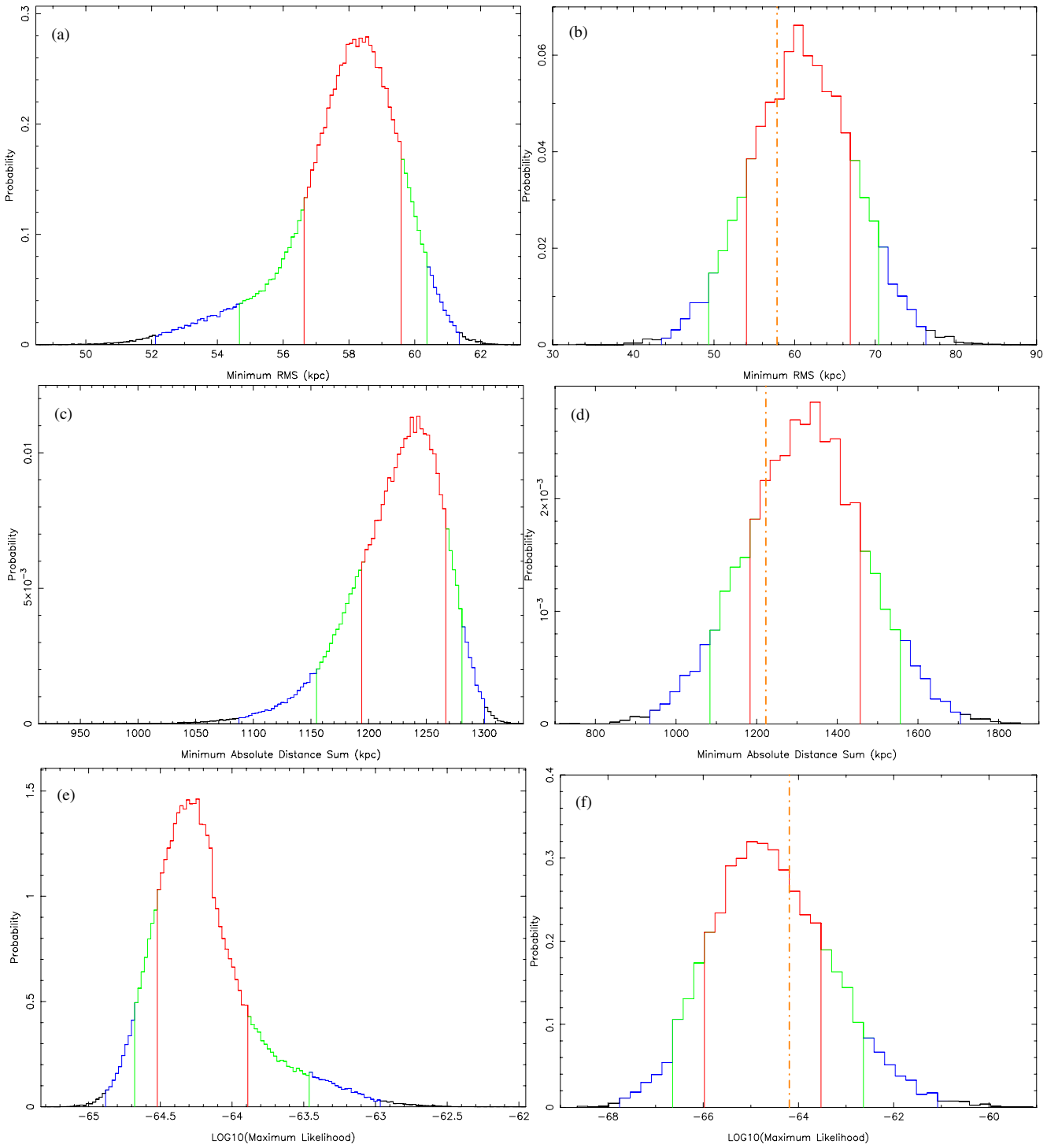

Figure 5. Probability distributions for the planarity of the entire satellite sample, as determined from three different measures of the plane goodness of fit. The left-hand column of figures gives the distribution of the goodness of fit statistic as obtained via plane fitting to 200,000 separate samplings of the *real* satellite sample. The right-hand column of figures summarizes the same procedure performed for 1000 separate samplings of each of 10,000 *random* realizations of the satellites (as per Section 2.2). It is important to note that each histogram in this column has been generated by plotting the *average* values from the 10,000 individual histograms corresponding to each of the random realizations and hence they should only be compared with the *average* of the histograms in the left-hand column. The goodness of fit statistic for (a) and (b) is the distribution rms; for (c) and (d) is the absolute distance sum and; for (e) and (f) is the sum of satellite likelihoods. The average of the histograms in (a), (c), and (e) are shown in (b), (d), and (f), respectively, as dashed lines. Red, green, and blue lines denote the extent of 1σ (68.2%), 90%, and 99% credibility intervals, respectively.

(A color version of this figure is available in the online journal.)

from Figure 1 and furthermore, if multiple planes of differing orientation are present as has been suggested for both the Milky Way's satellite system (e.g., Lynden-Bell 1982; Pawlowski et al. 2012b) and the M31 system (McConnachie & Irwin 2006), then the goodness of fit of the best-fit plane to the entire distribution is of little consequence. For this reason, we now concentrate our analysis on subsets or *combinations* of satellites. Specifically, we perform a pole-count analysis by determining the pole of

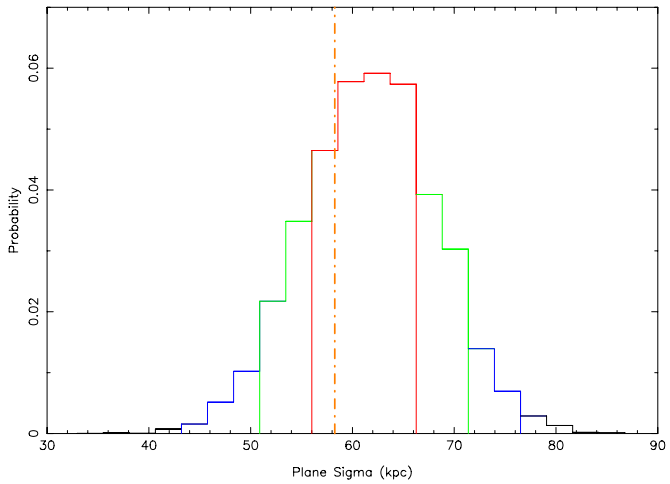

Figure 6. The probability distribution for the *average* 1σ width as determined from 10,000 random distributions of 27 satellites. This figure is generated from the same run as Figure 5(f) and is the result of marginalizing over the plane-orientation model parameters.

(A color version of this figure is available in the online journal.)

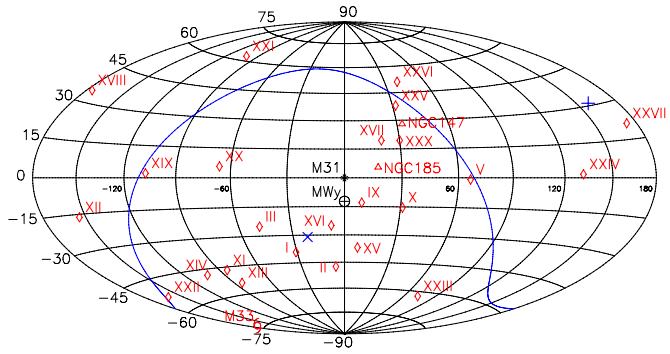

Figure 7. An Aitoff-Hammer projection showing the plane of maximum asymmetry identified from the full sample of best-fit satellite positions. It divides the distribution such that 21 satellites lie in one hemisphere, but only 6 in the other. The anti-pole of the maximum asymmetry plane lies just 28°.1 from the Milky Way as viewed from the center of M31.

(A color version of this figure is available in the online journal.)

the best-fit plane to every possible satellite combination of a particular size that can be drawn from the entire sample.

A pole-count analysis is an excellent way of mapping the degree of prominence of various planes that exist within the distribution as a whole, whatever their orientation may be. The choice of combination size is not trivial however. The number of combinations s of a particular number of satellites k that can be drawn from the entire sample of n satellites can be determined as follows:

$$s = \frac{n!}{k!(n-k)!} \tag{3}$$

For reasons that shall be discussed shortly, we will effectively be working with a sample of 25 satellite positions. It is clear from this equation, however, that with 25 satellites forming the entire sample, the total number of combinations that can be drawn may be very large, depending on the number of satellites forming the combinations. For instance, if $n = 25$ and $k = 13$, there are over 5.2 million possible combinations that can be drawn. Additionally, if we are to properly account for the uncertainties in the satellite positions, it will be necessary to sample from the distance distributions of each satellite a large number of times for every combination. Given that we must

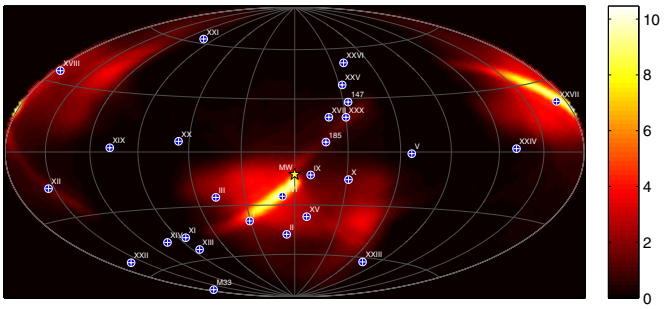

Figure 8. A pole density map showing the effective uncertainty in the location of the maximum asymmetry plane to the whole satellite sample. The poles of the maximum asymmetry planes derived for 200,000 possible realizations of the data are plotted, along with their corresponding anti-poles. The elongated distributions that run through the pole and anti-pole determined from the best-fit distribution (see Figure 7) arise due to the orientation of the uncertainty trails of the individual satellite positions, as presented in Figure 1. Note that the probability of the anti-pole of the asymmetry lying within a couple of degrees of the direction of the Milky Way is close to a maximum.

(A color version of this figure is available in the online journal.)

test every possible plane orientation (as per Section 2.1) for every rendition of every combination, the computation times can become impracticable. It is therefore necessary to limit our combination sizes as much as possible. We note, however, that the final pole-plot distribution showing the poles of the best-fit planes to each combination, is not so dependent on the combination size as might at first be thought.

With all the planes tested as per Section 2.1 having to pass through the center of M31, the minimum number of satellites that cannot be fitted exactly is three. This is therefore the smallest combination size we consider. There are 2300 combinations of three satellites that can be drawn from the full sample of 25 satellites. If we increase the combination size considerably to seven satellites, there are 480,700 satellite combinations that can be drawn. Due to an excessive number of combinations beyond this point, this is the largest combination size we consider. But it is critical to note that even if we produce our pole-plot map from combinations of only three satellites we *do not* exclusively find planes consisting of three satellites. If a plane of seven satellites exists for instance, then by Equation (3), such a plane will produce 35 poles at the same location on the pole plot, where a plane consisting of only three satellites would contribute only one pole. Conversely if we take combinations of seven satellites, despite the larger number of possible combinations in total, we become less sensitive to planes made up of less than seven satellites. So in a sense, the combination size we choose depends on the satellite planes we wish to be most sensitive to. In practice, we have found that the smaller combination sizes of three and four satellites are particularly useful for identifying the lowest rms planes congregating around the band of satellites visible in Figure 1. The larger combination sizes of five, six, and seven satellites gradually shift toward finding planes closer to the best-fit plane to the entire satellite sample illustrated in Figure 3.

Noting these points, we proceed as follows. First, the number of satellites per combination k is chosen ($3 \leqslant k \leqslant 7$) and then for each combination, distances are drawn for each of the satellites from their respective posterior distance distributions as provided in CIL12. To give a satisfactory representation of the form of the distributions, each combination is sampled 100 times. As such, each satellite combination contributes not 1 pole to the pole density map for the chosen combination size but 100, with

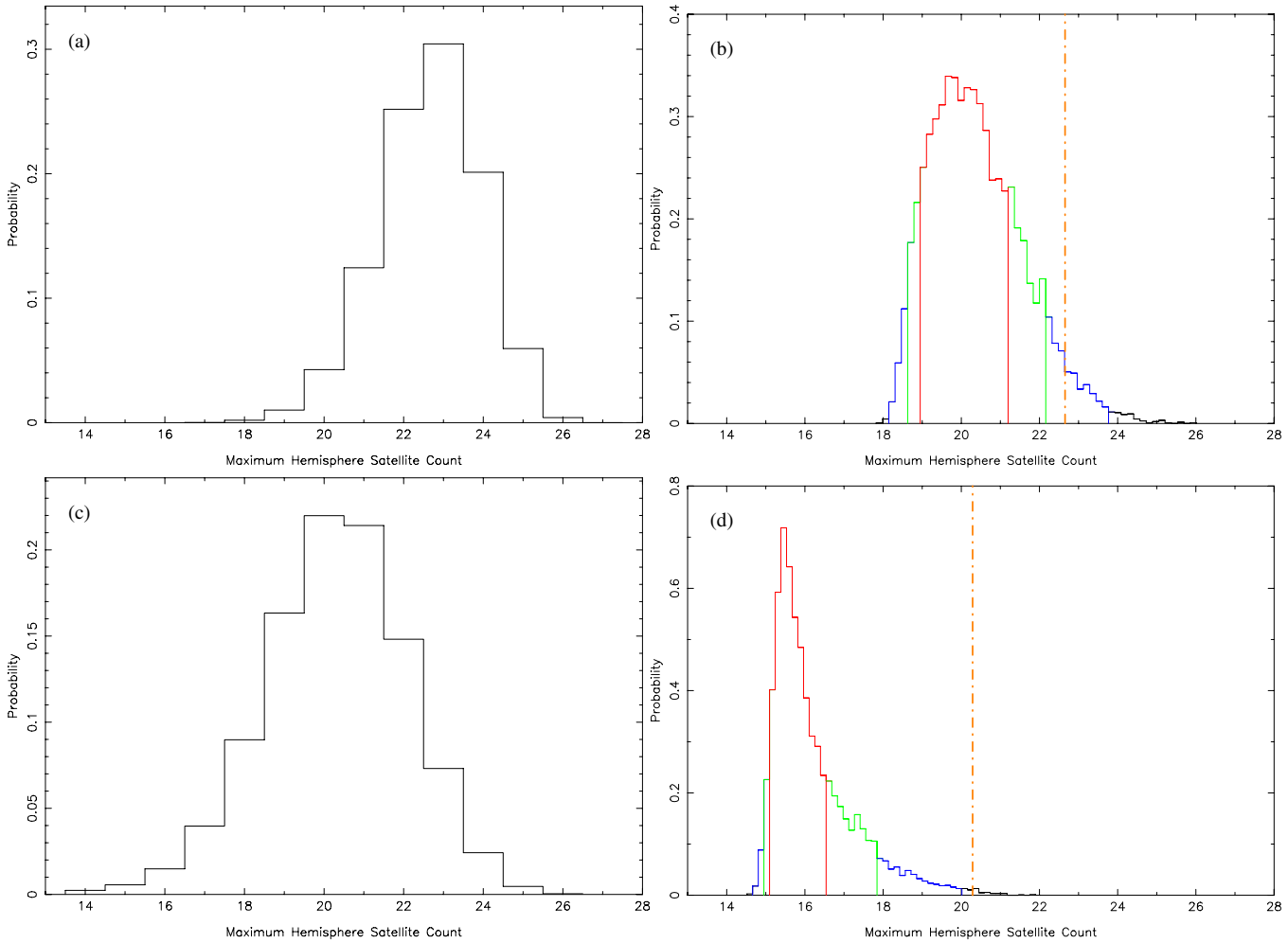

Figure 9. Asymmetry probability distributions. The top two histograms plot probability distributions for the greatest number of satellites that can be found in one hemisphere, as generated from (a) 200,000 samplings of satellite positions possible from the data and; (b) the *average* of 1000 samplings from each of 10,000 random realizations of the satellites generated as per Section 2.2. Figures (c) and (d) give the equivalent distributions when the maximum asymmetry plane is replaced with the fixed M31 tangent plane. As for Figure 5, the histograms in the right-hand column should only be compared with the average of the corresponding histogram in the left column. The average value of the histograms of (a) and (c) are shown in (b) and (d), respectively, as a dashed line.

(A color version of this figure is available in the online journal.)

the spread of poles relating the possible orientations of the best-fit plane to the combination, given the error in the individual satellite positions. The contribution of each pole to the density map is also weighted by dividing it by the rms of the best-fit plane it represents. Thus each pole does not contribute one count, but rather some fraction, depending on how good a fit the plane it represents is to the satellites in the combination. This fraction is also further divided by 100, since it represents only 1% of the samples for the combination, as just discussed.

As stated above, it should also be noted that we effectively limit the total number of satellites in our sample to 25 for all analysis in this subsection. This is to account for the bound group of satellites consisting of NGC 147, NGC 185, and And XXX (henceforth the NGC 147 group—see M. J. Irwin et al. 2013, in preparation). Since we suspect that these satellites orbit M31 as a group and since they all lie along the apparent plane identified in Figure 1, it is preferable to treat the group as a single object when we are not concerned with measurements of the significance of particular planes. To do this, we take the luminosity weighted center as an approximation for the center of mass, and treat this determined position as though it were the location of a single satellite. To calculate the luminosity weighted center, we can ignore the contribution from And XXX since it is negligible compared with the contributions of the two dwarf ellipticals. From the Third Reference Catalogue of Bright Galaxies (de Vaucouleurs et al. 1991), NGC 185 is 0.2 magnitudes brighter than NGC 147 in the V band. Each time the NGC 147 group is chosen as one of the "satellites" for a combination, distances to each of NGC 147 and NGC 185 are sampled from their respective distributions and the luminosity weighted center of the group is determined. As for any other combination, this position, along with all other satellites in the combination, is sampled 100 times.

The results of applying the above procedure to all combinations of three, four, five, six, and seven satellites that can be drawn from the total sample is presented in Figure 10. The left-hand column shows the fit to the most planar combination determined from the best-fit positions while the right-hand column shows the corresponding pole-density plots for all combinations of that particular number of satellites, based on 100 samples of each combination as per the discussion above. It is noteworthy that the best-fit planes to the most planar combinations are almost identical in every case, except for that of the three satellite combinations, where the rms values are so small for so many

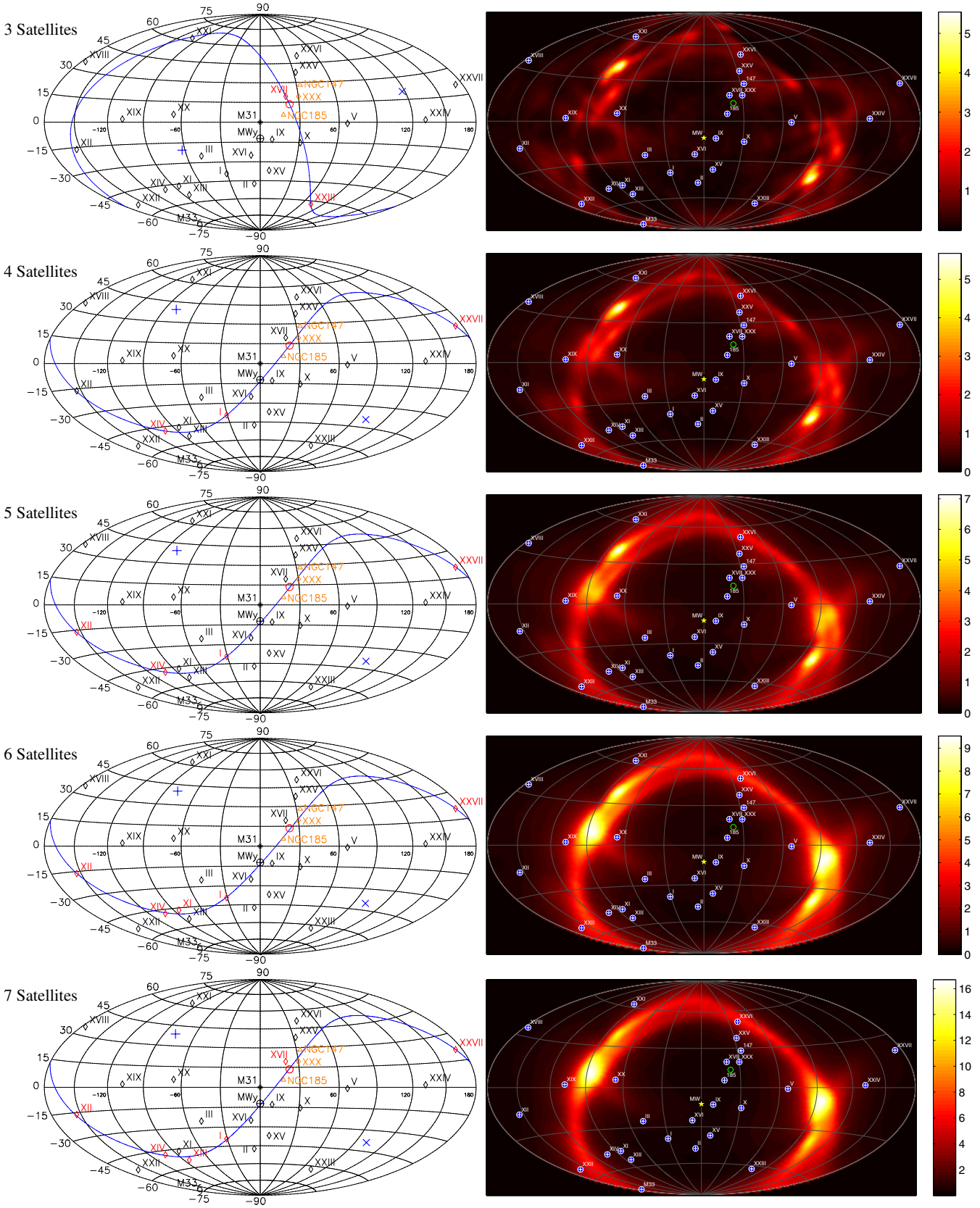

Figure 10. Best-fit planes and pole density maps for combinations of three through seven satellites. The left-hand column shows the best-fit plane through the combination of satellites that can be fit with the lowest rms. Satellites included in the best-fit combination are colored red. The center of the NGC 147 group is marked with a circle, and lies on the best-fit plane in every case. The three members of this group are colored orange. Only the best-fit satellite positions are considered for these plots. The right-hand column shows the corresponding pole-density plot for the poles of *all* satellite combinations. These plots have been weighted by the rms of each pole and fully account for the uncertainty in the satellite positions.

(A color version of this figure is available in the online journal.)

combinations as to make this result not particularly important. It should also be noted that these best-fit planes trace out the same approximate great circle as the prominent plane indicated in Figure 1, a result that shall be investigated a little later in Section 3.4. It is particularly interesting that the pole shared by each of these planes, located at $l_{\rm M31} \approx -80^\circ$, $b_{\rm M31} \approx 40^\circ$ corresponds to a pole count maximum in each of the pole plots. This indicates that many of the satellite combinations are aligned along this plane, hence further suggesting that the plane applies to more satellites than the combination sizes tested here. The other, lower latitude principle maximum in the pole plots is that corresponding approximately to the best fit to *all* the satellites and hence it grows more prominent in the plots made from larger combination sizes as discussed earlier.

Besides the pole count maxima that are strongly indicative of a highly planar subset of satellites, the other principle feature of the pole plots in Figure 10 is the great circle along which the pole count density is highest. This great circle is very prominent but great caution must be exercised in attributing any significance to it. It is centered on the Milky Way, indicating that the constituent poles result from a majority of satellites lying along the Earth to M31 line of site. But this reflects the anisotropy predicted from Figure 2, the result of the bias incurred by the finite area of the PAndAS survey. Hence it would seem that the progenitor of this prominent great circle is not physical but rather the result of selection effects. To further investigate the significance of the patterns observed in the pole plots, 1000 random realizations of 25 satellites were generated as per Section 2.2, and a similar pole count analysis performed on each of them. Specifically, the pole density distribution resulting from the best-fit planes to all combinations of five satellites was generated for each of them. The resulting pole plots for 8 of the 1000 random realizations (chosen at random) are presented in Figure 11 along with an enlarged version of the equivalent plot from Figure 10 generated from the real distribution. A bias toward a similar high-density great circle is indeed observed in these plots, but the plot generated from the actual data features a conspicuously narrower great circle, and a much more constrained distribution in general. This appears to be primarily the result of the large fraction of satellites that lie along the prominent plane that is repeatedly identified and plotted in the left-hand column of Figure 10. It should also be noted that this plane, while being oriented perfectly edge-on with respect to the Earth, contains a significant fraction of satellites lying well outside the region of the M31 sky where the detection bias is large, and hence it is unlikely that its prominence is due to our observational constraints.

Figure 12 provides for a comparison between the concentration of poles around the principle maximum in the pole distributions of the actual satellite distribution and the average of the 1000 random satellite distributions. From line (a) in Figure 12 we see that 21.5% of all combinations of the actual satellite positions are fitted by a best-fit plane with pole within 15° of the principal maximum (located at $l_{\rm M31} = -78\overset{\circ}{.}7$, $b_{\rm M31} = 38\overset{\circ}{.}4$). This is in stark contrast to the 12.0% that lie within 15° of the principal maximum for the average random realization of satellite positions (Figure 12, line (b)). Furthermore, we find that only 117 of the 1000 random realizations exhibited the degree of concentration of poles within 15° of the principal maximum that was observed for the actual satellite distribution. Hence it would seem that a large percentage of satellite combinations are fitted by best-fit planes that all have strikingly similar orientations when compared with what one could expect from a random distribution of satellites. Again, this points toward a significant plane of satellites that includes a large fraction of the whole satellite sample.

In order to obtain a better understanding of the satellites that this plane consists of, it is of particular interest to explore the number of times each satellite is included in a combination that is best fit by a plane with pole in close proximity to the principal maximum in the pole distribution for the entire sample. Once again, we use the pole distribution for all combinations of five satellites, and we count the number of times each satellite contributes to a pole within 3° of the principal maximum at $l_{\rm M31} = -78\overset{\circ}{.}7$, $b_{\rm M31} = 38\overset{\circ}{.}4$. The counts are divided by 100 to account for the 100 samples that are taken of each combination. The result can be seen in Figure 13. From this figure, it can be seen that the main contributors to the principal maximum in pole counts are those same satellites identified as forming a prominent plane in Figure 1, namely Andromedas I, XI, XII, XIII, XIV, XVI, XVII, XXV, XXVI, XXVII, and the NGC 147 group, along with Andromeda III and Andromeda IX. Hence the conclusion of our analysis thus far must be that there is indeed a significant plane in the satellite distribution of M31 and that it broadly consists of the aforesaid satellites. We therefore investigate the numerical significance of the best-fit plane to these satellites in Section 3.4. As yet there is still more to be gleaned from a study of the pole density distribution, however.

From Figure 13 we have been able to determine the principle contributing satellites to the principal maximum in the pole density distribution, but what of the remaining satellites? Do the positions of these satellites follow any particular trend? The best way to determine this is to construct pole-density plots of the two halves of the complete sample, namely the major contributors to the principal maximum and the minor contributors. The resulting pole plots are presented in Figure 14.

The left-hand plot of Figure 14 shows the pole density distribution generated from the major contributing satellites to the principal maximum at $l_{\rm M31} = -78\overset{\circ}{.}7$, $b_{\rm M31} = 38\overset{\circ}{.}4$. This half-sample includes Andromedas I, III, IX, XI, XII, XIII, XIV, XVI, XVII, XXV, XXVI, XXVII, and the NGC 147 group. As expected, this plot reflects the existence of the aforementioned plane with all combination poles lying in the vicinity of the principal maximum. The right-hand plot, with poles generated from the remaining 12 satellites, namely Andromedas II, V, X, XV, XVIII, XIX, XX, XXI, XXII, XXIII, XXIV, and M33, paints a very different picture, however. There is a much greater spread in the distribution of poles, with the great circle induced by the survey area bias once again conspicuous. Also prominent in this plot are two density maxima with their corresponding mirror images in the opposite hemisphere. The maximum lying midway between Andromedas XIX and XX lies very close to the pole of maximum detection bias at $l_{\rm M31} = -90^\circ$, $b_{\rm M31} = 0^\circ$ and so it is not unexpected, now that the prominent plane of satellites is effectively removed from the distribution. The elongated maximum passing through $l_{\rm M31} \approx 45^\circ$, $b_{\rm M31} \approx 45^\circ$ is more interesting, however, and suggests the possibility of a second plane, roughly orthogonal to the major plane represented in the left-hand plot, though much less conspicuous. The planes represented by this maximum pass close to the error trails on the M31 sky of Andromedas II, III, XIX, XX, XXIII, and XXIV. This maximum is faintly discernible in the pole distribution for combinations of six satellites presented in Figure 10 but is no more pronounced than anywhere else along the high-density great circle in any of the other pole plots. On account of this, it would appear that this plane is likely no more significant than

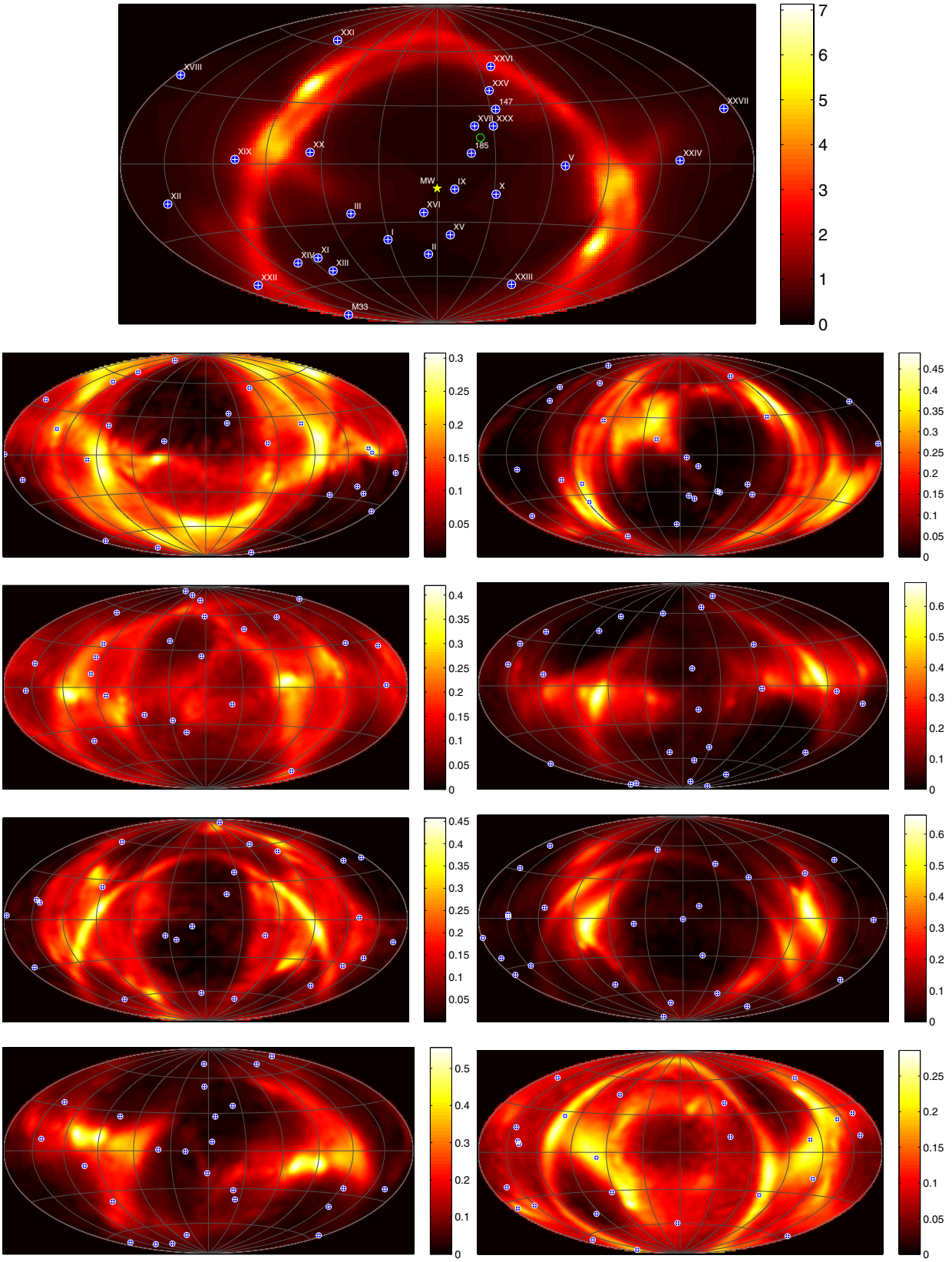

Figure 11. Pole density maps for eight random realizations of 25 satellites. The maps plot the poles for the best-fit planes to all combinations of five satellites. The contribution of each pole is weighted by the rms of the plane it represents. The map resulting from all combinations of five satellites drawn from the real data is shown again at the top for comparison. Great circle overdensities are evident to varying degrees in the plots and are a result of the satellite detection bias induced by the finite PAndAS survey area. Note that the density scale for the random realizations is much smaller than for the real data on account of the many realizations utilized for each combination of satellites from the real data.

(A color version of this figure is available in the online journal.)

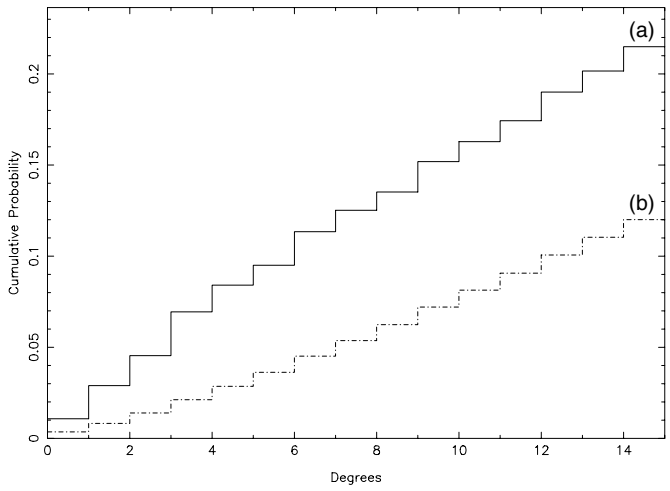

Figure 12. Radial density profiles showing the percentage of all poles lying within n degrees of the densest point in the pole count distributions (the principal maximum) for (a) the actual satellite distribution and (b) the average of 1000 random satellite distributions. The profile for the actual satellite distribution is generated from the same pole distribution as illustrated for five satellites in Figure 10 and at the top of Figure 11. Note that the relative linearity of (b) compared with (a) is simply a result of the averaging of a large number of individual profiles undertaken to produce the former.

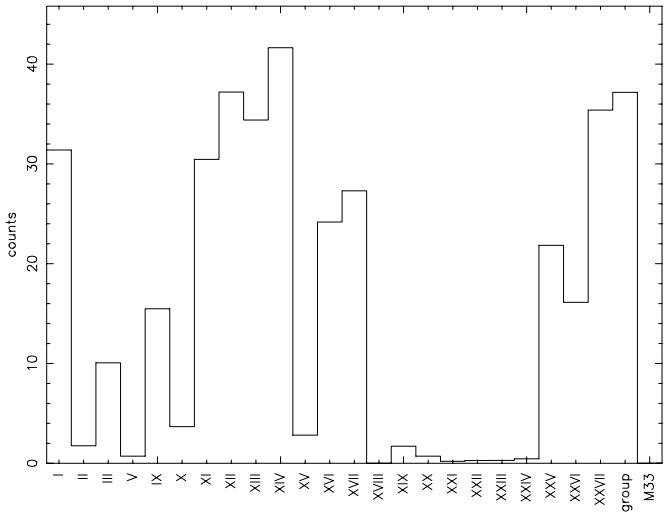

Figure 13. Histogram showing the relative contribution of each satellite to the pole density within 3° of the principal maximum at $l_{M31} = -78.^{\circ}7$, $b_{M31} = 38.^{\circ}4$. The histogram is generated from the same pole distribution as illustrated for five satellites in Figure 10 and at the top of Figure 11.

one would expect to find from a random satellite distribution subject to the same detection biases, such as those illustrated in Figure 11.

3.4. A Great Plane of Satellites

Throughout the investigation undertaken thus far, all evidence has repeatedly pointed toward a conspicuously planar subset of satellites consisting of roughly half the total sample of satellites. Andromedas I, XI, XII, XIII, XIV, XVI, XVII, XXV, XXVI, XXVII, and XXX as well as the dwarf ellipticals NGC 147 and NGC 185 all appeared to lie along a plane in Figure 1. The reality of this co-planarity was verified in Section 3.3 and in particular Figure 13, which also suggested that Andromeda III and Andromeda IX should be considered as plane members. Hence it is of great interest to ascertain whether this "great plane" is in fact significant. To do this, it is necessary to determine how likely such a plane is to arise from a random satellite distribution subject to the same selection biases. The plane itself and the satellites of which it is constituted are illustrated in Figure 15. The plane shown is that calculated from the best-fit satellite positions and has equation of the form: $0.158x + 0.769y + 0.620z = 0$ with pole at $(l_{M31}, b_{M31}) = (-78.^{\circ}4, 38.^{\circ}3)$. Note that for this section, we reinstate NGC 147, NGC 185, and Andromeda XXX as separate objects since we are again concerned with measurements of the significance of the planarity of the distribution. Our "great plane" thus consists of 15 satellites out of the entire sample of 27.

Using the method of Section 2.2, we again generate 10,000 independent random realizations of 27 satellites and seek the most planar combination of 15 satellites from each. For each random realization, we sample 1000 possible positions for each satellite as in previous sections and take the average value for the rms of the best-fit plane through the most planar combination. Since there are more than 17 million ways that 15 satellites can be drawn from 27, and since we are not concerned with the orientation of each fitted plane as we have been in all previous sections, we depart from the plane-fitting method of Section 2.1 for this section and instead proceed as follows. For each sample of satellite positions from each realization, 10,000 randomized planes are generated and the 15 closest satellites of the 27 to the plane are stored in each case and the rms recorded. The lowest rms achieved is hence taken to be that for the most planar combination of 15 satellites in the sample. These minimum rms values from each of the 1000 samples of the particular random realization are then averaged to provide the best representation for the realization, given the distance uncertainties. Figure 16 provides probability distributions in the rms for the observed "great plane" (a) together with those for the average rms for the most planar combination from each random realization (b). The average rms for the observed plane is plotted in (b) for comparison.

As can be seen from Figure 16, the rms for the observed plane is very low compared to what one could reasonably expect from a chance alignment. Indeed, the average rms of 12.58 kpc for the observed plane is found to be equaled or exceeded in only 36 out of the 10,000 random realizations. The chances of obtaining such a planar group of 15 satellites from a sample of 27 at random is thus estimated as 0.36%. Hence we can conclude from this test that the observed plane is very unlikely to be a chance alignment, but rather the result of some underlying physical mechanism. Note that an independent but equivalent investigation is presented in ILC13 where such an alignment is found to occur in only 0.15% of instances. This is due to the larger central obstruction adopted in that analysis (19.6 versus 7.9 deg^2) which rejects more satellites in close proximity to the plane pivot point (M31) where small plane distances are most likely.

4. DISCUSSION

Throughout the analysis conducted in Section 3, the presence of a prominent plane of satellites has been a consistent feature. This is not the first time that a significant plane of satellites has been identified from among the denizens of the M31 halo however. As early as 1995, Fusi Pecci et al. (1995) had noted that the majority of the then known satellites lay conspicuously in a plane oriented edge-on with respect to the Milky Way. Koch & Grebel (2006) identified a highly significant plane lying within 5°–7° of being polar. Furthermore, they identify a subset of nine

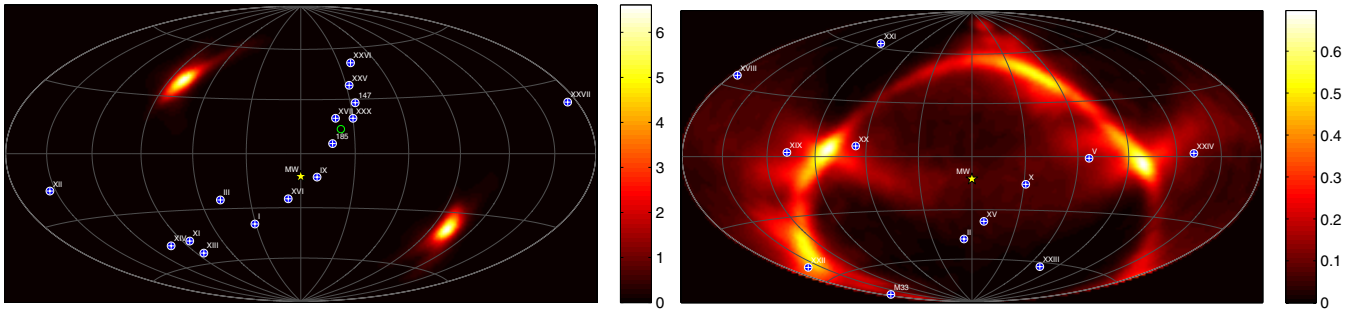

Figure 14. Pole density distributions generated from all combinations of five satellites possible from: (left) the satellites contributing significantly to the principal maximum at $l_{M31} = -78.^{\circ}7$, $b_{M31} = 38.^{\circ}4$ as per Figure 13 and (right) the remaining 12 satellites.

(A color version of this figure is available in the online journal.)

satellites from this plane lying within a thin disk with an rms of 16 kpc. Metz et al. (2007) and later Metz et al. (2009a) similarly identify a disk of satellites, this time not so markedly polar, with pole (in our coordinate system) at $(l_{M31}, b_{M31}) = (-70.^{\circ}2, 32.^{\circ}9)$. They find this disk to have an rms height of 39.2 kpc. This disk is clearly the same structure that we identify here, being tilted by only $8.^{\circ}6$ with respect to our "great plane." Our plane is found to have a much smaller rms of just $12.34^{+0.75}_{-0.43}$ kpc, however, despite including a comparable number of satellites. It is particularly noteworthy, however, that their satellite sample is significantly different from that used here, with their disk including M32, NGC 205, IC10, LGS3, and IC1613—all of which lie outside the portion of the PAndAS survey region used in this study (see Figure 10(c) of CIL12). Indeed, it is clear from Figure 4 of McConnachie & Irwin (2006) that the galaxies M32, IC10, LGS3, and IC1613 all lie along the same great circle as our "great plane" in Figure 15, as do their entire error trails. Their conformity along with Andromeda I to a thin disk is noted in the said paper as one of eight possible "streams of satellites," thus providing another early detection of the plane identified by this study. Both Majewski et al. (2007) and Irwin et al. (2008) also draw attention to the linear distribution of many of the plane-member satellites on the sky, a consequence of the edge-on orientation of the plane as indicated by the present study. The plane of Metz et al. (2009a) does however include a significant number of satellites that, while included in our sample, we exclude due to their looser association with our plane. This then accounts for the much smaller rms height observed in our study.

Unlike previous studies of the M31 satellite system, we have a significant advantage in this study on account of the greatly improved sample of satellites available to us. Our sample is not only more numerous, but the positions are all determined via the same method applied to the same data as per CLI11 and CIL12. We are thus afforded unprecedented knowledge of the satellite detection biases, as well as the uncertainties in the object positions, and have factored this knowledge into the analysis. An understanding of this bias is of particular importance when it comes to ascertaining the significance of any substructure identified, since a physically homogeneous satellite distribution will inevitably appear anisotropic after "folding in" the selection function and it is important that we do not attribute physical significance to this anisotropy.

Even after taking these effects into account, however, there can be little doubt that the plane described in Section 3.4 is a real physical object. The component satellites extend well into the regions of low detection bias in Figure 2 and the analysis of the last section makes it clear that such a thin disk

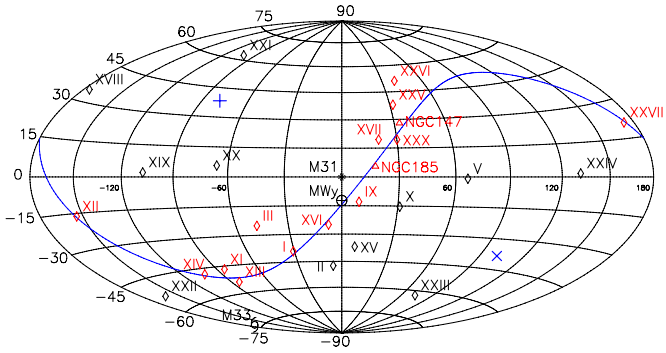

Figure 15. A Great Plane of Satellites consisting of Andromedas I, III, IX, XI, XII, XIII, XIV, XVI, XVII, XXV, XXVI, XXVII, XXX, NGC 147, and NGC 185. The plane shown is that derived from the best-fit satellite positions. The pole is located at $(l_{M31}, b_{M31}) = (-78.^{\circ}4, 38.^{\circ}3)$.

(A color version of this figure is available in the online journal.)

of satellites has very little chance of arising within a random satellite distribution of the same size, even when subject to the same observation biases. Furthermore, it should be noted that the study of the plane's significance in Section 3.4 is likely to be conservative, given that if the satellites M32, IC10, LGS3, IC1613, and NGC 205 were to be included in the analysis, the significance of our observed plane would likely grow still further. What is also particularly interesting is that subsequent research has shown 13 of the 15 objects to be co-rotating. This result is discussed in more detail in ILC13.

What then could be the progenitor of this "great plane"? The polar orientation one might expect to arise had the satellites formed within the dark matter halo or had the dynamical friction proposed by Quinn & Goodman (1986) had sufficient time to take effect is not observed. Similarly, the findings of Metz et al. (2009b) seemingly preclude the possibility that the structure might be the result of the accretion of an external galactic association. Furthermore, there is apparently no marked distinction in the metallicities of the disk members compared with the non-disk members as one might expect from this scenario, though it is possible that some of the non-disk satellites may share the same origin as the disk members. There remains, however, the possibility that the satellites trace out the tidal debris of a galaxy merger. This is a particularly interesting possibility, especially since the plane, when projected onto the M31 tangent plane, is in close alignment with the Giant Stellar Stream. Indeed, Hammer et al. (2010) show that the Giant Stellar Stream could feasibly be the product of a major merger event

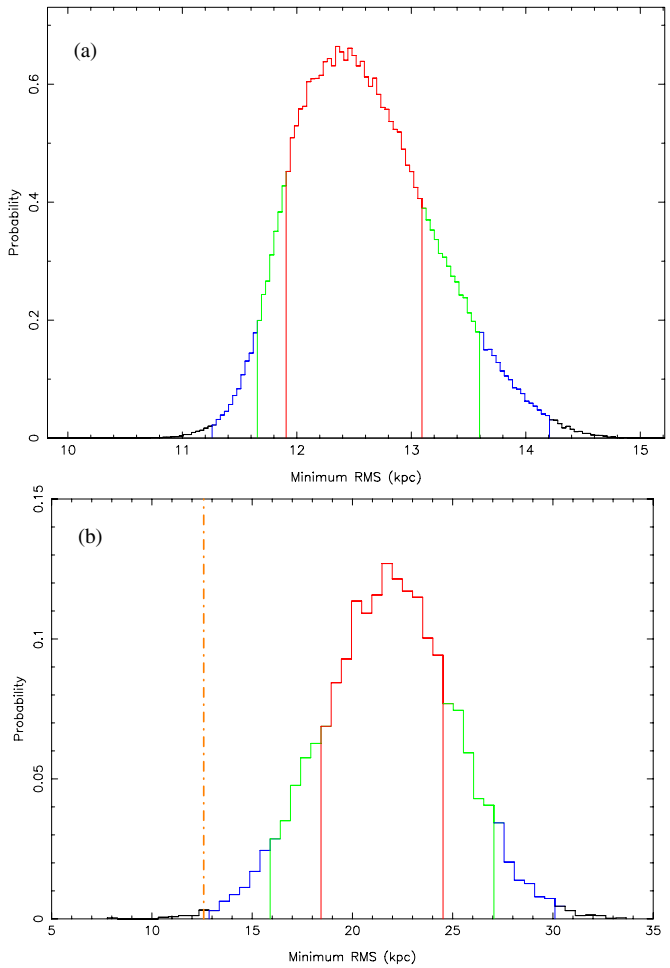

Figure 16. Determining the significance of the observed "great plane" of satellites (see Figure 15). Figure (a) gives the distribution of possible values of the rms obtainable from 200,000 realizations of possible positions of the 15 plane members, given their respective distance probability distributions. Figure (b) plots the *average* rms of the best-fit plane through the most planar combination of 15 satellites for each of 10,000 random realizations of 27 satellites. These satellites are subject to the same selection biases as the real data. As for Figure 5, histogram (b) should only be compared with the average of histogram (a), which is plotted in (b) as a dashed line. It is thus clear that the planarity observed for our "great plane" of satellites is very unlikely to arise by chance. The 1σ (68.2%), 90%, and 99% credibility intervals are shown as red, green, and blue lines, respectively.

(A color version of this figure is available in the online journal.)

that began around 9 Gyr ago, sustained by the returning stars from a tidal tail oriented similarly to our "great plane."

If a link is to be established, the observed asymmetry of the system must also be compatible with the tidal scenario however. It is of particular interest that, of the 13 co-rotating satellites in the plane, all but one lie on the near side of the M31 tangent plane. Indeed, if we removed all of the plane member-satellites from the system, the remaining satellite distribution would no longer be significantly asymmetric. With almost all of the satellites currently on the near side of M31, it would seem on first consideration that the progenitor event could not have occurred substantially more than a typical orbital time ago or else the satellites would have had sufficient time to disperse. This suggests the event responsible must have occurred within the last 5 Gyr. Other studies, however, have supported the proposition that a group of tidal dwarf galaxies could survive for extended periods while retaining the asymmetry inherent from the time of their formation. For instance, Duc et al. (2011) find three moderately old tidal dwarf candidates with this asymmetry preserved. It must also be remembered that the precise orbits of the satellites are undetermined and so it is not clear how close they have come to M31 in the past. As discussed by Pawlowski et al. (2011), there is also evidence that tidal material can survive in a "bridge" between the interacting galaxies for an extended period. Nevertheless, it must be cautioned that there is no established precedent for tidal dwarfs with the longevity implied by the stellar populations of the M31 satellites, and the fact that they continue to adhere to such a thin structure is even more perplexing under such a scenario.

There is also another striking characteristic of the observed plane. As one will note from examination of Figure 15 (and indeed the left-hand column of plots in Figure 10), it is oriented perfectly edge-on with respect to the Milky Way. While there is a noted bias toward detection of satellites positioned along planes oriented in this way, it must be remembered that this bias arises primarily due to the propensity for detecting satellites close to the line of sight passing through M31. Many of the satellites observed to lie on our plane are located a good distance from this line of sight, however, and well into the low-bias portions of the M31 sky. In any case, the random realizations of Section 3.4 suffer from the same biases and yet show unequivocally that the observed plane is very unlikely to arise by chance. Hence if we are to accept these results, we must also accept the plane's orientation.

Further to this strikingly edge-on orientation, it is also noteworthy that the plane is approximately perpendicular to the Milky Way disk. This fact can be easily seen if the constituent satellites are traced out in Galactic coordinates (i.e., all lie on approximately the same Galactic longitude). This of course raises the question—how does the orientation of the Milky Way's polar plane of satellites compare with this plane? Noting that the average pole of the "Vast Polar Structure" described by Pawlowski et al. (2012b) points roughly in the direction of M31, the two planes are approximately orthogonal. These precise alignments are discussed in more detail in ILC13, but suffice to say here that this alignment is particularly interesting and suggests that the Milky Way and M31 halos should not necessarily be viewed as fully isolated structures. It is entirely conceivable that our current ignorance as to the coupling between such structures may be to blame for our inability to pin down the precise mechanism by which such planes arise.

Finally, in consequence of these findings, most particularly with respect to the highly significant, very thin disk of satellites that has been identified, it is clear that if ΛCDM is to remain the standard model of cosmology, the occurrence of such structures has to be explicable within it. The possible deeper implications of the satellite anisotropies are discussed in Kroupa et al. (2010), Angus et al. (2011), Fouquet et al. (2012), and Kroupa (2012), wherein other alternative cosmologies are also highlighted.

5. CONCLUSIONS

It is clear that while the satellites of M31 when taken as a whole are no more planar than one can expect from a random distribution, a subset consisting of roughly half the sample *is* remarkably planar. The presence of this thin disk of satellites has been conspicuous throughout the analysis contained in this paper. The degree of asymmetry determined from the satellite distribution is also found to be relatively high. Of particular note, the orientation of the asymmetry is very significant, being aligned very strongly in the direction of the Milky Way. When

this fact is combined with the apparent orthogonality observed between the Milky Way and M31 satellite distributions and the Milky Way disk, it appears that the two halos may in fact be coupled. Regardless, the great plane of satellites identified in this study, and its clear degree of significance, is not directly expected from ΛCDM cosmology. This finding provides strong evidence that thin disks of satellites do indeed exist in galaxy halos, and whether or not the standard model can account for such structures remains to be seen.

A.R.C. thanks Macquarie University for their financial support through the Macquarie University Research Excellence Scholarship (MQRES) and both the University of Sydney and Université de Strasbourg for the use of computational and other facilities. G.F.L. thanks the Australian Research Council for support through his Future Fellowship (FT100100268) and Discovery Project (DP110100678). R.A.I. and D.V.G. gratefully acknowledge support from the Agence Nationale de la Recherche though the grant POMMME (ANR 09-BLAN-0228). Based on observations obtained with MegaPrime/MegaCam, a joint project of CFHT and CEA/DAPNIA, at the Canada–France–Hawaii Telescope (CFHT), which is operated by the National Research Council (NRC) of Canada, the Institut National des Science de l'Univers of the Centre National de la Recherche Scientifique (CNRS) of France, and the University of Hawaii.

REFERENCES

Angus, G. W., Diaferio, A., & Kroupa, P. 2011, MNRAS, 416, 1401
Conn, A. R., Ibata, R. A., Lewis, G. F., et al. 2012, ApJ, 758, 11 (CIL12)
Conn, A. R., Lewis, G. F., Ibata, R. A., et al. 2011, ApJ, 740, 69 (CLI11)
de Vaucouleurs, G. 1958, ApJ, 128, 465
de Vaucouleurs, G., de Vaucouleurs, A., Corwin, H. G., Jr., et al. 1991, Third Reference Catalogue of Bright Galaxies (Berlin: Springer)
Duc, P.-A., Cuillandre, J.-C., Serra, P., et al. 2011, MNRAS, 417, 863
Fouquet, S., Hammer, F., Yang, Y., Puech, M., & Flores, H. 2012, in SF2A-2012: Proc. Annual Meeting of the French Society of Astronomy and Astrophysics, ed. S. Boissier et al. (Paris: SF2A), 333
Fusi Pecci, F., Bellazzini, M., Cacciari, C., & Ferraro, F. R. 1995, AJ, 110, 1664
Hammer, F., Yang, Y. B., Wang, J. L., et al. 2010, ApJ, 725, 542
Hartwick, F. D. A. 2000, AJ, 119, 2248
Holmberg, E. 1969, ArA, 5, 305
Ibata, R. A., Lewis, G. F., Conn, A. R., et al. 2013, Natur, 493, 62 (ILC13)
Irwin, M. J., Ferguson, A. M. N., Huxor, A. P., et al. 2008, ApJL, 676, L17
Knebe, A., Gill, S. P. D., Gibson, B. K., et al. 2004, ApJ, 603, 7
Koch, A., & Grebel, E. K. 2006, AJ, 131, 1405
Kroupa, P. 2012, PASA, 29, 395
Kroupa, P., Famaey, B., de Boer, K. S., et al. 2010, A&A, 523, A32
Kroupa, P., Theis, C., & Boily, C. M. 2005, A&A, 431, 517
Libeskind, N. I., Frenk, C. S., Cole, S., et al. 2005, MNRAS, 363, 146
Lovell, M. R., Eke, V. R., Frenk, C. S., & Jenkins, A. 2011, MNRAS, 413, 3013
Lynden-Bell, D. 1976, MNRAS, 174, 695
Lynden-Bell, D. 1982, Obs, 102, 202
Lynden-Bell, D., & Lynden-Bell, R. M. 1995, MNRAS, 275, 429
Majewski, S. R., Beaton, R. L., Patterson, R. J., et al. 2007, ApJL, 670, L9
McConnachie, A. W., & Irwin, M. J. 2006, MNRAS, 365, 902
McConnachie, A. W., Irwin, M. J., Ibata, R. A., et al. 2009, Natur, 461, 66
Metz, M., Kroupa, P., & Jerjen, H. 2007, MNRAS, 374, 1125
Metz, M., Kroupa, P., & Jerjen, H. 2009a, MNRAS, 394, 2223
Metz, M., Kroupa, P., & Libeskind, N. I. 2008, ApJ, 680, 287
Metz, M., Kroupa, P., Theis, C., Hensler, G., & Jerjen, H. 2009b, ApJ, 697, 269
Navarro, J. F., Abadi, M. G., & Steinmetz, M. 2004, ApJL, 613, L41
Palma, C., Majewski, S. R., & Johnston, K. V. 2002, ApJ, 564, 736
Pawlowski, M. S., Kroupa, P., Angus, G., et al. 2012a, MNRAS, 424, 80
Pawlowski, M. S., Kroupa, P., & de Boer, K. S. 2011, A&A, 532, A118
Pawlowski, M. S., Pflamm-Altenburg, J., & Kroupa, P. 2012b, MNRAS, 423, 1109
Quinn, P. J., & Goodman, J. 1986, ApJ, 309, 472
Springel, V., Wang, J., Vogelsberger, M., et al. 2008, MNRAS, 391, 1685
Starkenburg, E., Helmi, A., De Lucia, G., et al. 2013, MNRAS, 429, 725
Vera-Ciro, C. A., Sales, L. V., Helmi, A., et al. 2011, MNRAS, 416, 1377
Zentner, A. R., Kravtsov, A. V., Gnedin, O. Y., & Klypin, A. A. 2005, ApJ, 629, 219